Platelet glycoprotein Ibα forms catch bonds with human WT vWF but not with type 2B von Willebrand disease vWF

Tadayuki Yago,[1] Jizhong Lou,[2,3] Tao Wu,[4] Jun Yang,[4,5] Jonathan J. Miner,[1] Leslie Coburn,[2] José A. López,[6,7] Miguel A. Cruz,[8] Jing-Fei Dong,[8] Larry V. McIntire,[2] Rodger P. McEver,[1,9] and Cheng Zhu[2,3,4]

[1]Cardiovascular Biology Research Program, Oklahoma Medical Research Foundation, Oklahoma City, Oklahoma, USA. [2]Coulter Department of Biomedical Engineering, [3]Institute for Bioengineering and Biosciences, and [4]Woodruff School of Mechanical Engineering, Georgia Institute of Technology, Atlanta, Georgia, USA. [5]Mechanical and Materials Engineering Department, University of Western Ontario, London, Ontario, Canada. [6]Puget Sound Blood Center, Seattle, Washington, USA. [7]Department of Medicine, University of Washington, Seattle, Washington, USA. [8]Thrombosis Research Section, Department of Medicine, Baylor College of Medicine, Houston, Texas, USA. [9]Department of Biochemistry and Molecular Biology, University of Oklahoma Health Sciences Center, Oklahoma City, Oklahoma, USA.

Arterial blood flow enhances glycoprotein Ibα (GPIbα) binding to vWF, which initiates platelet adhesion to injured vessels. Mutations in the vWF A1 domain that cause type 2B von Willebrand disease (vWD) reduce the flow requirement for adhesion. Here we show that increasing force on GPIbα/vWF bonds first prolonged ("catch") and then shortened ("slip") bond lifetimes. Two type 2B vWD A1 domain mutants, R1306Q and R1450E, converted catch bonds to slip bonds by prolonging bond lifetimes at low forces. Steered molecular dynamics simulations of GPIbα dissociating from the A1 domain suggested mechanisms for catch bonds and their conversion by the A1 domain mutations. Catch bonds caused platelets and GPIbα-coated microspheres to roll more slowly on WT vWF and WT A1 domains as flow increased from suboptimal levels, explaining flow-enhanced rolling. Longer bond lifetimes at low forces eliminated the flow requirement for rolling on R1306Q and R1450E mutant A1 domains. Flowing platelets agglutinated with microspheres bearing R1306Q or R1450E mutant A1 domains, but not WT A1 domains. Therefore, catch bonds may prevent vWF multimers from agglutinating platelets. A disintegrin and metalloproteinase with a thrombospondin type 1 motif–13 (ADAMTS-13) reduced platelet agglutination with microspheres bearing a tridomain A1A2A3 vWF fragment with the R1450E mutation in a shear-dependent manner. We conclude that in type 2B vWD, prolonged lifetimes of vWF bonds with GPIbα on circulating platelets may allow ADAMTS-13 to deplete large vWF multimers, causing bleeding.

Introduction

When blood vessels are disrupted, circulating platelets adhere to exposed subendothelial surfaces through interactions of platelet glycoprotein Ibα (GPIbα) with its ligand vWF, which is immobilized on collagen fibers (1). This is the first step in a cascade of adhesion and signaling events that produce a hemostatic plug at the injured site. Dysregulated interactions between GPIbα and vWF cause bleeding in disorders such as von Willebrand disease (vWD) and thrombosis in disorders such as thrombotic thrombocytopenic purpura (2–7).

vWF is a multimeric plasma glycoprotein with up to 80 subunits. The mature vWF subunit has 2,050 residues with multiple A-, B-, C-, and D-type domains (8). The A1 domain contains the binding site for platelet GPIbα (9, 10). GPIbα has a 289-residue N-terminal domain composed of 8 tandem leucine-rich repeats (GPIbαN) and a long O-glycosylated stalk, followed by a transmembrane domain and a cytoplasmic tail (11, 12). Crystallographic studies reveal that the leucine-rich repeats of GPIbαN wrap around one side of the A1 domain of vWF but that only the β-finger region on the N-terminal side and the β-switch region on the C-terminal side make contact with A1 (13, 14).

To bind GPIbα, vWF must be subjected to high fluid shear, treated with modulators such as botrocetin or ristocetin, or immobilized to collagen (15). Mutations in the A1 domain that cause type 2B vWD increase binding of vWF to GPIbα with low concentrations of a modulator. Paradoxically, this gain of function in binding of vWF to GPIbα is associated with excessive bleeding (7, 15–17). The structural basis for the gain of function and the type 2B vWD phenotype is not understood.

Platelet adhesion and aggregation require that GPIbα and vWF interact under dynamic conditions of blood flow, which exerts hydrodynamic forces on GPIbα/vWF bonds (18). Plasma vWF agglutinates circulating platelets only when they are exposed to pathologically high shear flow such as in stenotic arteries (15). Platelets tether to and roll on immobilized vWF, but do not firmly adhere (1). Counterintuitively, flow enhances rather than impedes platelet adhesion, despite the dislodging forces (1, 19). Mutations in vWF may change the mechanical regulation of platelet adhesion. For example, the I1309V substitution in the A1 domain (20) causes 1 type 2B vWD mutant to slow its dissociation from GPIbα and to support rolling of more platelets at slower velocities without a minimum shear requirement (21). In the present study, we demonstrated other examples of type 2B vWD mutants with similar effects.

Nonstandard abbreviations used: ADAMTS-13, a disintegrin and metalloproteinase with a thrombospondin type 1 motif–13; AFM, atomic force microscopy; GPIb, glycoprotein Ib; PSGL-1, P-selectin glycoprotein ligand–1; SMD, steered molecular dynamics; vWD, von Willebrand disease.

Conflict of interest: The authors have declared that no conflict of interest exists.

Citation for this article: *J. Clin. Invest.* **118**:3195–3207 (2008). doi:10.1172/JCI35754.

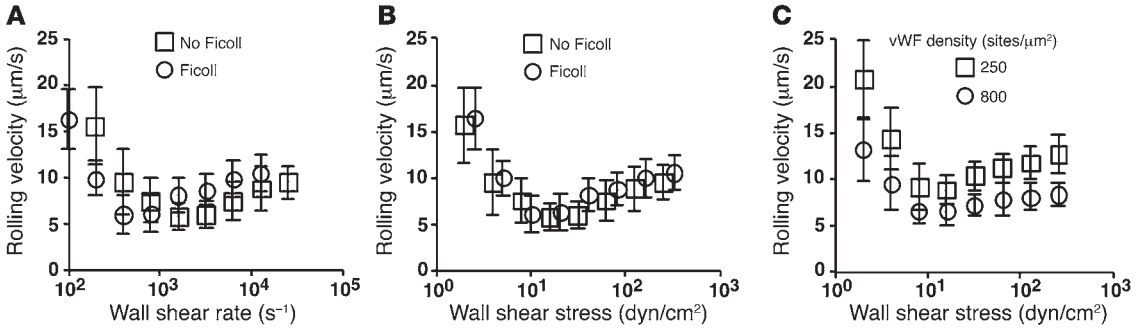

Figure 1
Platelets roll on different vWF site densities with biphasic velocity curves that align with wall shear stress but not with wall shear rate. Platelets suspended in medium without or with 6% Ficoll were perfused through a flow chamber containing immobilized vWF in a range of flow rates. The flow chamber was coated with 100 μg/ml (**A**–**C**) or 440 μg/ml (**C**) vWF, resulting in the site densities shown in **C**. The rolling velocity is plotted versus the wall shear rate (**A**) or wall shear stress (**B** and **C**). Data are mean ± SD of 5 experiments.

Whereas interactions of GPIbα with vWF mediate platelet rolling on disrupted vascular surfaces, interactions of selectins with their glycoconjugate ligands mediate leukocyte rolling on inflamed vascular surfaces (5). The functional similarities in these receptor/ligand systems suggest similarities in their biophysical characteristics. Indeed, both GPIbα/vWF and selectin/ligand interactions have rapid on-rates (21–23) and rapid off-rates (19, 21, 23–25). Of particular interest, both interactions support flow-enhanced adhesion (26). Importantly, applied force affects the lifetimes of selectin/ligand bonds in distinct ways (27, 28). As force initially increases from low levels, lifetimes increase (catch bonds) until a maximal value is reached. As force increases further, lifetimes decrease (slip bonds). Catch bonds between L-selectin and its ligands govern flow-enhanced leukocyte rolling (29). As flow increases from suboptimal levels, leukocytes roll more slowly and more regularly until a minimal rolling velocity is reached. As flow increases further, transitions to slip bonds cause rolling velocities to increase (29). A substitution that alters the hinge between the lectin and EGF domains of L-selectin affects catch bonds by prolonging bond lifetimes at low forces. This mutation lowers the shear threshold requirement for L-selectin–mediated rolling and causes flowing microspheres bearing the mutant L-selectin to agglutinate with flowing leukocytes that express L-selectin ligands (30). A substitution in the ligand-binding surface of L-selectin also prolongs bond lifetimes at low forces and eliminates the shear threshold for leukocyte rolling (31). These findings prompted us to investigate whether the similarities between the GPIbα/vWF and selectin/ligand systems extend to these new areas.

Here we show that GPIbα formed catch bonds with WT vWF. Mutations in the vWF A1 domain that cause type 2B vWD converted catch bonds to slip bonds by prolonging bond lifetimes at low forces. Steered molecular dynamics (SMD) simulations of GPIbα dissociating from the A1 domain suggested mechanisms for catch bonds and their conversion. Catch bonds governed flow-enhanced platelet rolling on immobilized vWF, which may prevent agglutination of circulating platelets by plasma vWF. Our findings provide insights into the pathogenesis of type 2B vWD.

Results

Platelets roll on vWF with biphasic velocity curves that align with wall shear stress, but not with wall shear rate. We used high-speed video microscopy at 250 frames per second (fps) to measure velocities of platelets rolling or translocating on immobilized vWF over a wide range of flow rates in a flow chamber. Rolling velocity first decreased with increasing flow, despite the increasing dislodging force (Figure 1), a feature of flow-enhanced leukocyte rolling mediated through L-selectin/ligand interactions (29) that had not to our knowledge been previously described for platelet rolling mediated through GPIbα/vWF interactions. As rolling velocities decreased, the platelets rolled more uniformly, with longer stop times, more frequent stops, and more rolling steps with complete stops with 0 velocity (data not shown); these rolling behaviors reflect more stable adhesion (29). After reaching a minimum velocity, further increases in flow increased rolling velocity (Figure 1) and reversed the above trends in rolling behavior (data not shown), which is intuitive and has been observed previously (19). We measured rolling velocities in medium with or without 6% Ficoll, which changes viscosity — and hence wall shear stress and tether force — by 2.6-fold without changing wall shear rate (29). The rolling velocity and rolling behavior curves did not align when plotted versus wall shear rate (Figure 1A and data not shown), but collapsed into single curves when plotted versus wall shear stress (Figure 1B and data not shown). This scaling rule excluded shear rate–dependent transport as a mechanism for the observed flow-enhanced rolling and suggested that shear stress, and hence force applied to adhesive bonds, may account for this phenomenon. Flow-enhanced rolling at low shear was observed even at very high vWF density (800 sites/μm²; Figure 1C), produced by using a vWF coating concentration equal to or higher than those used in previous studies (19). This suggests that the previous failure to observe flow-enhanced platelet rolling was not due to differences in the density of immobilized vWF.

As force increases, GPIbα forms catch bonds and then slip bonds with WT A1, but forms only slip bonds with R1306Q A1 and R1450E A1. Leukocytes rolling through interactions of L-selectin with its ligands also exhibit biphasic velocity curves that scale with wall shear stress (29). Catch bonds between L-selectin and its ligands govern flow-enhanced leukocyte rolling, where rolling velocities decline with increasing but still low flows. At higher flows, catch bonds transition to slip bonds, causing rolling velocities to increase (29). The basis for this causal relationship is the stop-and-go pattern of rolling, which is slower when the stop period is longer because of the longer bond lifetime. Since this argument seems applicable to platelet rolling, we hypothesized that transitions from catch to slip bonds between GPIbα and vWF govern the biphasic rolling curves observed in Figure 1. To test this hypothesis, we used atomic force microscopy (AFM) to measure how force affected lifetimes of bonds of GPIbα with the vWF A1

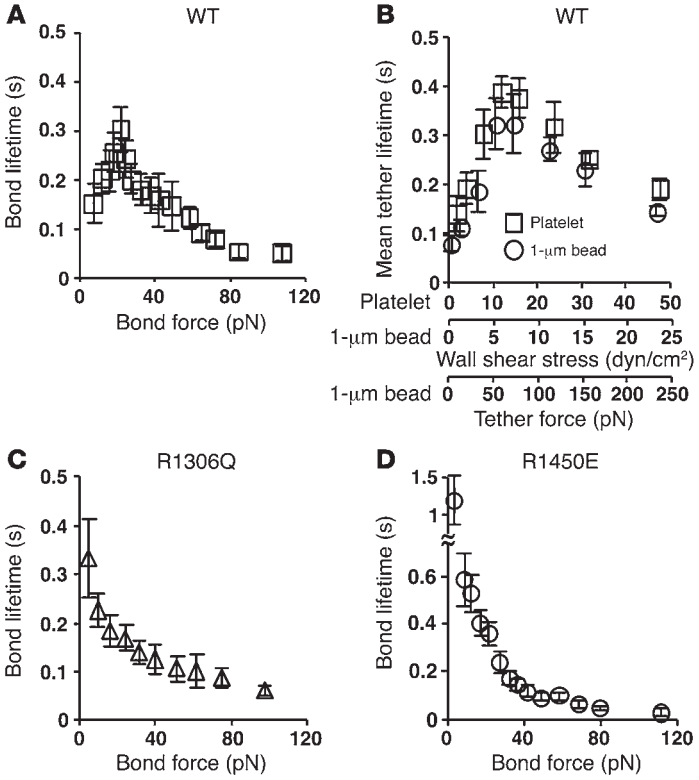

Figure 2

As force increases, GPIbα forms catch bonds and then slip bonds with WT A1, but forms only slip bonds with R1306Q A1 and R1450E A1. (**A**, **C**, and **D**) Lifetimes of single GPIbα bonds with WT A1 (**A**), R1306Q A1 (**C**), or R1450E A1 (**D**) were measured by AFM. Data are mean ± SEM of several tens of measurements for each point. (**B**) Lifetimes of platelets or 1-μm-radius microspheres bearing GPIbα transiently tethered to a flow chamber floor coated with 2 μg/ml WT A1 were measured. Data are mean ± SD of 3 experiments.

domain. A large number of mostly single-bond lifetimes were measured to derive the mean lifetime — the reciprocal off-rate $1/k_{off}$ for first-order dissociation of single bonds — over a range of forces (27, 28). Lifetimes of GPIbα/A1 bonds exhibited a biphasic pattern characteristic of transition from catch to slip bonds (Figure 2A) (27, 28). The mean lifetime increased with increasing force, indicating catch bonds, until an optimal force was reached where lifetime reached a maximum. Thereafter, the mean lifetime decreased with increasing force, indicating slip bonds. To confirm this unusual phenomenon, we measured force-dependent lifetimes (4-ms resolution) of platelets or 1-μm-radius microspheres bearing GPIbα transiently tethered to low-density vWF A1 that did not support rolling or skipping in a flow chamber. Transitions from catch to slip bonds were observed (Figure 2B). Indeed, the mean transient tether lifetime versus wall shear stress curves for platelets and microspheres had identical shapes and aligned well after doubling the *x* axis scale of the platelet curve relative to the *x* axis scale of the microsphere curve, which allows for conversion of wall shear stress into tether force (see Methods). The biphasic lifetime versus wall shear stress curves were reciprocally related to the rolling velocity versus wall shear stress curves in Figure 1. This is analogous to the reciprocal relationship between the biphasic L-selectin/ligand bond lifetime versus wall shear stress curves and the leukocyte rolling velocity versus wall shear stress curves (29–31). This reciprocal relationship is intuitive because a rolling platelet must dissociate its rearmost GPIbα/vWF bond to move a step forward. Thus, longer bond lifetimes cause slower rolling velocities.

We also studied 2 mutations in the vWF A1 domain: R1306Q and R1450E. The former occurs in some patients with type 2B vWD (32), whereas the latter was designed to mimic the gain-of-function phenotype of type 2B vWD (33–35). GPIbα is thought to bind to these gain-of-function mutants of A1 with higher affinity than to WT A1 (13, 35). Consistent with these previous observations, the bond lifetimes of R1306Q A1 and R1450E A1 dissociating from GPIbα at low forces were much longer than those of WT A1 (Figure 2, C and D). Remarkably, the lifetimes of GPIbα bonds with R1306Q (Figure 2C) or R1450E (Figure 2D) decreased monotonically with increasing force. Thus, the catch bonds observed between GPIbα and WT A1 in the low-force regime were converted to slip bonds between GPIbα and the mutant A1 proteins, which continued as slip bonds above the optimal force, at which GPIbα/WT A1 catch bonds transition to slip bonds. At these higher forces, the lifetimes of slip bonds between GPIbα and WT A1 or R1306Q A1 were not measurably different, but those between GPIbα and R1450E A1 were longer. These results suggest that the altered force dependence of GPIbα/A1 dissociation may explain the phenotype in type 2B vWD.

Unfixed and fixed platelets roll with biphasic velocity curves on WT A1, but with monophasic velocity curves on R1306Q A1 and R1450E A1. We next determined that the biphasic velocity curves observed when platelets rolled on intact vWF (Figure 1) also occurred when platelets rolled on the isolated A1 domain. On WT A1, platelets exhibited biphasic rolling velocity curves that did not align with wall shear rate (Figure 3A) but did align with wall shear stress (Figure 3B). These data confirmed that isolated A1 domain adsorbed on a surface is sufficient to mediate flow-enhanced platelet rolling (10). Furthermore, the biphasic rolling velocity curves (Figure 3B) mirrored the biphasic bond lifetime curve obtained with WT A1 (Figure 2B). The hypothetical relationship between these 2 sets of curves predicts that the velocity curves of platelet rolling on R1306Q A1 and R1450E A1 should also mirror the respective bond lifetime curves in Figure 2, C and D, i.e., increase monotonically with increasing flow. Indeed, no flow enhancement was observed for platelet rolling on either A1 mutant. Compared with rolling velocities on WT A1, those on either A1 mutant were slow at low flows and gradually increased as flow increased (Figure 3, C–F). Furthermore, platelets rolled more slowly on R1450E A1 than on R1306Q A1, which corresponds to the longer bond lifetimes of R1450E A1 than R1306Q A1 at matched forces. These data further support the causal relationship between rolling velocity and bond lifetime.

A possible mechanism for flow to reduce platelet rolling velocity on vWF is increased number of GPIbα/vWF bonds. This is because the bond force tethering a rolling platelet to the surface has 2 components that are proportional to each other. The component along the flow direction balances the hydrodynamic force, whereas the component perpendicular to the flow direction compresses the platelet against the wall. Higher flows cause larger compressive forces, which may enlarge the contact area with the wall, enabling more bond formation. This is different from and much larger than the compressive force on a flowing platelet when it contacts the surface with a sharp approach angle, which is required to push the mass center away from the surface as the discoid-shaped platelet pivots over the contact point (36). The hypothetical enlarge-

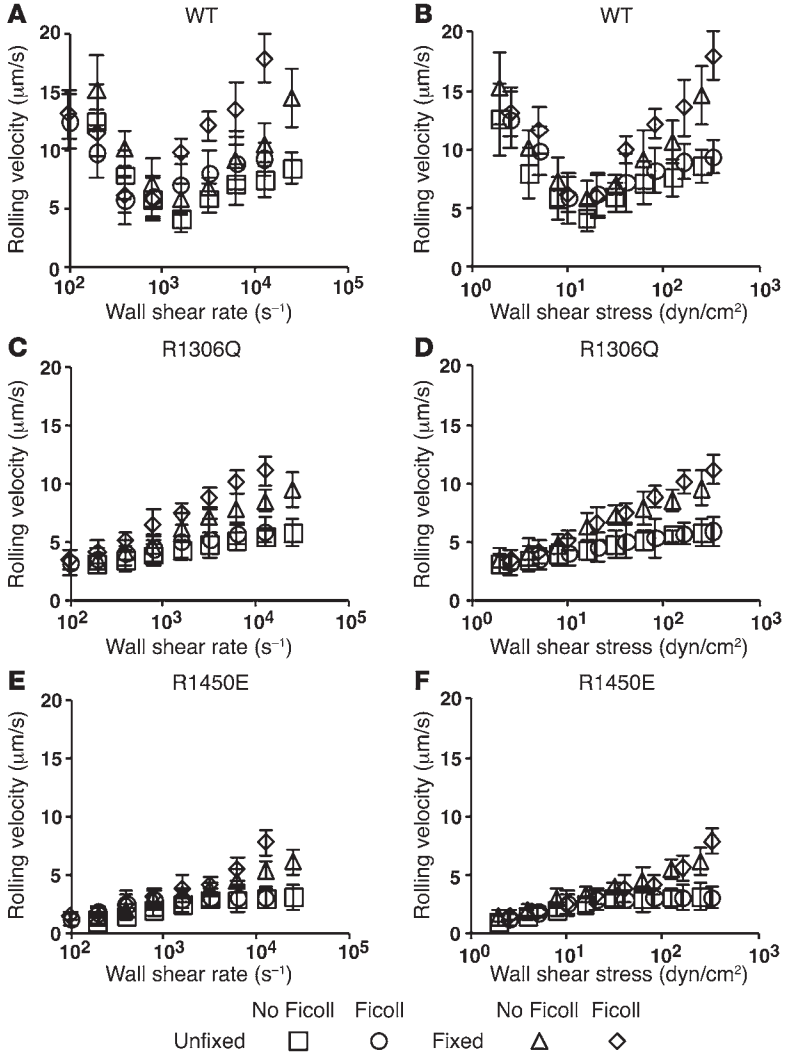

Figure 3

Unfixed and fixed platelets roll with biphasic velocity curves on WT A1, but with monophasic velocity curves on R1306Q A1 and R1450E A1. Unfixed or fixed platelets in medium without or with Ficoll (to increase the viscosity by 2.6-fold) were perfused through a flow chamber containing immobilized WT A1 (**A** and **B**), R1306Q A1 (**C** and **D**), or R1450E A1 (**E** and **F**) in a range of flow rates. The rolling velocity is plotted versus the wall shear rate (**A**, **C**, and **E**) or wall shear stress (**B**, **D**, and **F**). Data are mean ± SD of 5 experiments.

ment of contact area by compressive force predicts alignment of the rolling velocity curves when plotted against wall shear stress rather than wall shear rate; indeed, we observed this in Figures 1 and 3 (unfixed platelets). To test this hypothesis further, we fixed platelets with paraformaldehyde, which likely prevented global deformation and extrusion of membrane tethers (37). Compared with unfixed platelets, fixed platelets rolled slightly faster, especially at higher wall shear stresses (Figure 3). However, the qualitative shapes of the curves, biphasic for WT A1 and monophasic for both A1 mutants, did not change. These data demonstrated that platelet deformation and/or extrusion of membrane tethers exert a moderate influence on rolling velocities at higher shear stresses. Platelet deformation cannot be the dominant mechanism underlying flow-enhanced rolling, because eliminating deformability did not alter the descending phase of the velocity curve for rolling on WT A1.

Velocity curves of GPIbα-bearing microspheres rolling on WT or mutant A1 mimic those of platelets and align when plotted versus tether force. To extend the transient tether lifetime measurements shown in Figure 2B, we measured rolling velocities of microspheres bearing GPIbα to exclude influences of cellular features, including the discoid shape of platelets, on rolling behavior. The microsphere velocity curves were qualitatively similar to the respective platelet velocity curves for rolling on WT A1 and on the 2 A1 mutants (Figure 4). Microsphere rolling velocities were more sensitive to flow change, but the shapes of the curves remained the same. The biphasic velocity curves of GPIbα microspheres rolling on WT A1 confirmed that flow-enhanced rolling does not require specific cellular features.

The spherical shape of microspheres allowed us to determine the tether force acting on the GPIbα/vWF bonds linking a rolling microsphere to the chamber floor (see Methods). Microspheres of 1-μm radius have a similar size to platelets. Increasing the microsphere radius to 3 μm increases the tether force by 9-fold at the same wall shear stress (29). As expected, changing the microsphere size shifted the rolling velocity curves, but did not change their qualitative shapes (Figure 4). When plotted versus wall shear rate, curves of microspheres of different sizes in media of different viscosities did not align (Figure 4, A, D, and G). When plotted versus wall shear stress, curves of microspheres of the same size in media of different viscosities aligned, but those of microspheres of different sizes remain separated (Figure 4, B, E, and H). When plotted versus tether force, all curves collapsed regardless of the microsphere size and medium viscosity (Figure 4, C, F, and I). This scaling rule applied to the data for WT A1 and for the 2 A1 mutants, regardless of the qualitative shapes (biphasic for WT A1 and monophasic for the mutants) and the quantitative aspects (ascending more rapidly for R1306Q than for R1450E) of the curves. L-selectin/ligand-mediated tether lifetimes of microspheres obey the same scaling rule: curves align when plotted versus tether force, but do not align when plotted versus wall shear rate or wall shear stress (29). This is expected for L-selectin/ligand bonds as well as GPIbα/vWF-A1 bonds because force, rather than shear rate or shear stress, is applied to molecular bonds. Taken together, our data indicate that the dissociation kinetics of GPIbα/vWF A1 bonds govern platelet rolling velocities and that catch bonds specifically govern flow-enhanced platelet rolling.

Flowing platelets agglutinate with microspheres bearing R1306Q A1 or R1450E A1, but not with microspheres bearing WT A1. Despite its presence in plasma, multimeric vWF normally does not agglutinate circulating platelets unless it is immobilized at sites of vascular injury or exposed to extremely high shear rate (~20,000 s^{-1}), like that in stenotic arteries (15, 38). However, plasma vWF may spontaneously interact with platelet GPIbα in patients with type 2B vWD (16, 17, 39). We hypothesized that GPIbα/vWF catch bonds prevent inappropriate platelet agglutination, yet allow platelet rolling on

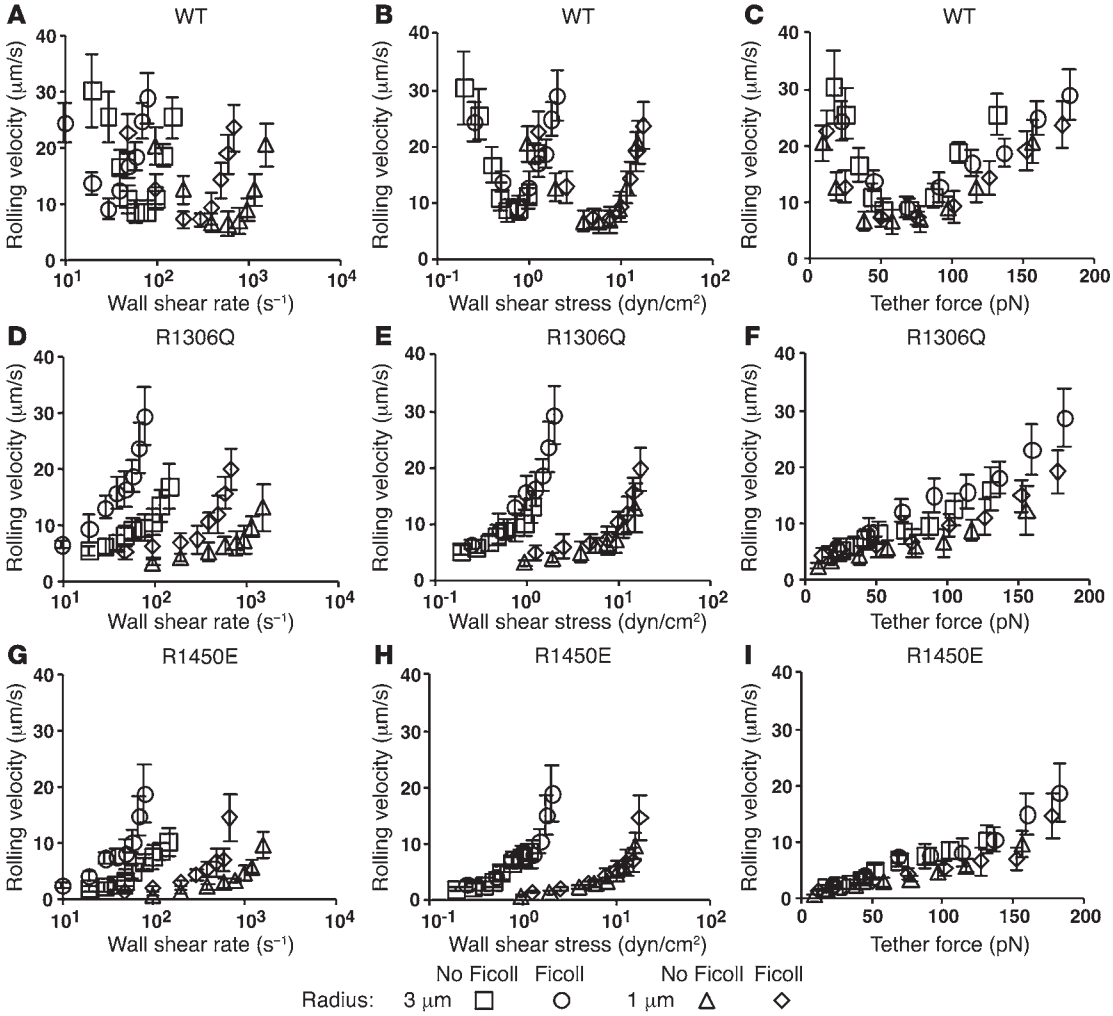

Figure 4
Velocity curves of GPIbα-bearing microspheres rolling on WT or mutant A1 mimic those of platelets and align when plotted versus tether force. GPIbα-bearing microspheres of 3- or 1-μm radius in medium with or without Ficoll (to increase the viscosity by 2.6-fold) were perfused through a flow chamber containing immobilized WT A1 (**A**–**C**), R1306Q A1 (**D**–**F**), or R1450E A1 (**G**–**I**) in a range of flow rates. The rolling velocity is plotted versus the wall shear rate (**A**, **D**, and **G**), wall shear stress (**B**, **E**, and **H**), or tether force (**C**, **F**, and **I**). Data are mean ± SD of 5 experiments.

injured vessel walls. This hypothesis can be understood by comparing the force exerted on bonds linking platelets in a circulating aggregate to that tethering a rolling platelet to a stationary wall. It follows from fluid mechanics theory that the former (40) is much smaller than the latter (41), because the blood velocity is small relative to fast-flowing platelets but large relative to slow-rolling platelets. In the catch bond regime, lower forces yield shorter lifetimes, whereas larger forces yield longer lifetimes. When plotted versus wall shear rate, the velocity curves for platelets rolling on intact vWF or WT A1 domain were superimposed (Figure 5A). After doubling the *x* axis scale of the platelet curves relative to the *x* axis scale of the curve of GPIbα-bearing microspheres of 1-μm radius, the descending phases of these curves nearly aligned, suggesting that the tether forces applied to microspheres of 1-μm radius, which are roughly the size of platelets, were no more than 2-fold different from the tether forces of platelets, despite their different shapes. This allowed us to use the 1-μm-radius microsphere data to estimate forces on platelets in the catch bond regime as we did for the transient tether lifetime data (Figure 2B). At an arterial shear rate of 1,000 s^{-1}, the average tensile force between 2 1-μm microspheres in a flowing doublet is 6.2 pN (Figure 5B) (40), too small for a GPIbα/A1 bond to last long enough to support a stable doublet (Figure 2, A and B). Yet at the same wall shear rate, an approximately 15-fold higher force is required to tether a 1-μm-radius microsphere to the flow chamber floor (Figure 5B and Methods), high enough to elicit GPIbα/A1 catch bonds that support rolling (Figure 2, A and B). This hypothesis is consistent with our observation that extremely high shear stresses promoted platelet agglutination because the engagement of GPIbα/vWF catch bonds prolonged their lifetimes at higher forces. It also explains the observed platelet agglutination in some patients with type 2B vWD, because longer bond lifetimes at low forces (Figure 2, C and D) should promote platelet agglutination at normal arterial shear rates.

To test our hypothesis, we perfused platelets with FITC-labeled A1-bearing 3-μm-radius microspheres in a flow chamber coated with HSA, which does not support platelet adhesion, at a wall

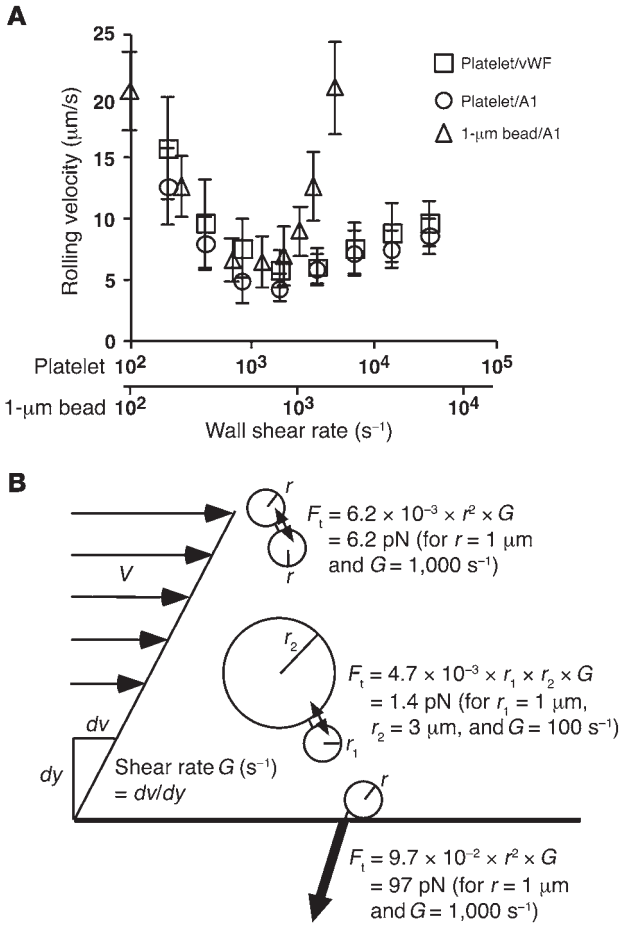

Figure 5
At the same shear rate, tensile force applied to bonds that link flowing platelets or microspheres is much lower than that applied to bonds that tether rolling platelets or microspheres. (**A**) Platelets or GPIbα-bearing microspheres of 1-μm radius were perfused through a flow chamber containing immobilized vWF or WT A1. The rolling velocity is plotted versus the wall shear rate. Data are mean ± SD of 5 experiments. (**B**) Schematic showing tensile forces (F_t) between spheres of equal and unequal size in a doublet as well as between a sphere and the wall under a simple shear field.

shear rate of 100 s^{-1}. At this wall shear rate, the average tensile force between a 1-μm-radius microsphere and a 3-μm-radius microsphere in a flowing doublet is 1.4 pN (Figure 5B) (40). Samples collected at the flow chamber exit were fixed and stained by PE-labeled anti-CD61 mAb to identify platelets. Flow cytometry revealed very few particles containing fluorescence markers for both platelets and microspheres bearing WT A1 (percent of particles with significantly increased fluorescence intensity, 0.7% ± 0.3%, mean ± SD of 4 experiments; Figure 6A), but many particles labeled for both platelets and microspheres bearing R1306Q A1 (13% ± 5%, mean ± SD of 3 experiments; Figure 6B) or R1450E A1 (33% ± 7%, mean ± SD of 4 experiments; Figure 6C). Addition of anti-GPIbα mAb blocked agglutination, which confirmed that it was mediated by specific interactions of GPIbα with A1 (Figure 6, B and C). Fluorescence microscopy confirmed that few platelets agglutinated with WT A1 microspheres (Figure 6D), whereas many platelets agglutinated with microspheres bearing R1450E (Figure 6E) or R1306Q (data not shown). Agglutination did not develop in the presence of anti-GPIbα mAb (Figure 6F). These data support our hypothesis that catch bonds prevent agglutination of flowing platelets and that loss of catch bonds causes circulating platelets to agglutinate spontaneously, as observed in patients with type 2B vWD.

A disintegrin and metalloproteinase with a thrombospondin type 1 motif–13 reduces platelet agglutination with microspheres bearing R1450E A1A2A3-triplet. Hydrodynamic forces acting on spontaneously agglutinated platelets in the circulation are applied to multimeric vWF that crosslinks the platelets (Figure 5B), which are much larger than the forces applied to vWF in the plasma. The increased force may make vWF more susceptible to proteolytic cleavage by the plasma metalloprotease a disintegrin and metalloproteinase with a thrombospondin type 1 motif–13 (ADAMTS-13) (42–44). To test this hypothesis, FITC-labeled 3-μm-radius microspheres were coated first with A1A2A3-triplet containing WT or R1450E A1 and then coated with or without ADAMTS-13. Microspheres were mixed with platelets and perfused through a flow chamber coated with HSA at a range of wall shear rates. Samples collected at the flow chamber exit were fixed and stained by PE-labeled anti-CD61 mAb to identify platelets. Similar to the experiments using microspheres bearing A1, flow cytometry revealed very few particles containing fluorescence markers for both platelets and microspheres bearing WT A1A2A3, but many particles labeled for both platelets and microspheres bearing R1450E A1A2A3 (Figure 6G), which suggested that isolated A1 domain and the A1A2A3-triplet behave similarly. Addition of anti-GPIbα mAb blocked agglutination, confirming that it was mediated by specific interactions of GPIbα with A1A2A3. As the wall shear rate increased, platelet agglutination increased with microspheres bearing WT A1A2A3 but decreased with microspheres bearing R1450E A1A2A3 (Figure 6G). This is consistent with our observation that GPIbα formed catch bonds with WT A1 but slip bonds with R1450E A1 in this force range; the average tensile force between a 1-μm-radius microsphere and a 3-μm-radius microsphere in a flowing doublet is 28 pN for a shear rate of 2,000 s^{-1}. It is evident from Figure 6G that ADAMTS-13 reduced platelet agglutination with microspheres bearing R1450E A1A2A3 at higher wall shear rates. These data support our hypothesis and suggest a molecular mechanism for type 2B vWD (see Discussion).

Structural explanations for why GPIbα forms catch bonds with WT A1 but not with R1306Q and R1450E A1. What is the atomic-level structural basis for GPIbα/vWF catch bonds? The 2 crystal structures of GPIbαN:A1 complexes (13, 14) provide little insight because they were obtained in the absence of force. Therefore, we used SMD simulations to study the GPIbαN:A1 structure as it changes over time in response to applied forces. We performed 2 sets of simulations using 2 GPIbαN:A1 cocrystal structures as starting points: the first set used a complex between WT GPIbαN and WT A1 (14), and the second used a mutant complex between M349V GPIbαN and R1306Q A1 (13). Key observations from the first set are depicted in Figure 7 (see also Supplemental Video 1; supplemental material available online with this article; doi:10.1172/JCI35754DS1), which is representative of 2 simulations. In the crystal structure, A1 residue D1269 forms a salt bridge with R1306 and possibly with R1450. GPIbαN contacts A1 via the β-switch and via the β-finger (Figure 7A). This equilibrated structure was used as a starting point (0 ns) to generate the simulated structures in Figure 7, B–E, by pulling at the C_α atom of GPIbα C-terminal residue L267 via a spring

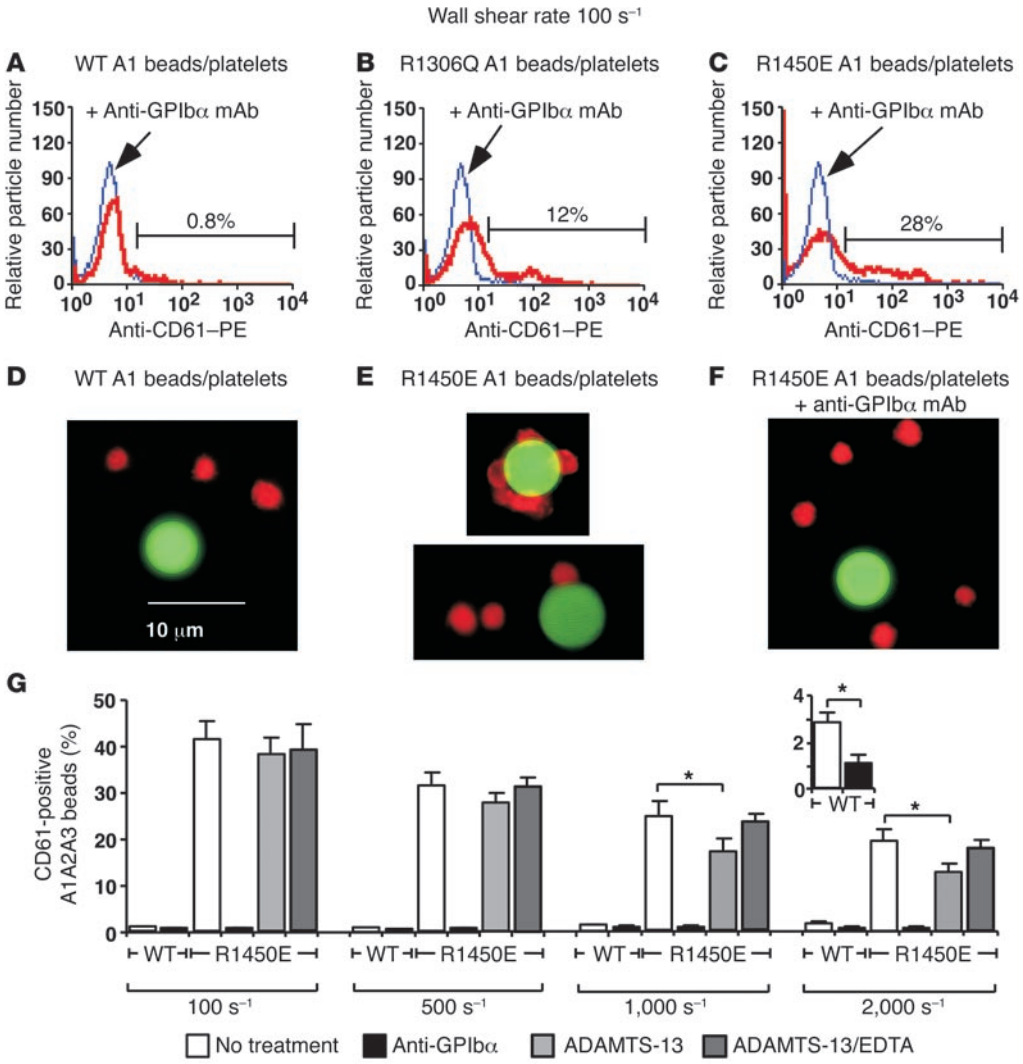

Figure 6

Flowing platelets agglutinate with microspheres bearing R1306Q A1 or R1450E A1 (and R1450E A1A2A3), but not with microspheres bearing WT A1 (and A1A2A3), allowing ADAMTS-13 to cleave R1450E A1A2A3. Mixtures of platelets and Yellow-Green–labeled microspheres coated with WT A1 (**A** and **D**), R1306Q A1 (**B**), or R1450E A1 (**C**, **E**, and **F**) or with WT A1A2A3 or R1450E A1A2A3 domain triplet and then incubated with or without ADAMTS-13 (**G**) were perfused through a flow chamber coated with HSA in medium without or with 20 μg/ml anti-GPIbα mAb. After exiting the flow chamber, suspensions were fixed, stained with PE-conjugated anti-CD61 mAb, and analyzed by flow cytometry (**A**–**C** and **G**) or by fluorescence microscopy (**D**–**F**). (**A**–**C**) Flow cytometry of samples gated for single green particles. The red fluorescence histograms measured without (red curve) or with (blue curve) anti-GPIbα mAb are compared. The percentage of particles in the anti-GPIbα mAb curve with significant increase in fluorescence intensity relative to the curve without this mAb is indicated for 1 experiment; the mean ± SD of 3 or 4 experiments is shown in Results. (**D**–**F**) Representative fluorescence micrographs of mixtures of platelets and microspheres bearing WT A1 (**D**), R1450E A1 (**E**), or R1450E A1 plus anti-GPIbα mAb (**F**). Scale bar: 10 μm. (**G**) Percentage (mean ± SD of 3 experiments) of single green particles with red fluorescence, as measured by flow cytometry after the samples prepared as indicated were subjected to different shears. Inset shows the WT groups subjected to shear rate of 2,000 s^{-1} on a smaller scale. *$P < 0.01$, Student's *t* test.

(~700 pN/nm constant) that moved horizontally to the right at a constant speed of 0.5 nm/ns with the C_α atom of the A1 N-terminal residue H1268 harmonically constrained. At 5 ns, the salt bridge between D1269 and R1306/R1450 ruptured, which extended the A1 N-terminal sequence and rotated the A1 counterclockwise by 11° (Figure 7B). At 9.4 ns, further pulling forced the GPIbα β-finger to slide over A1, enabling the formation of a salt bridge between GPIbα E14 and A1 R1334 (Figure 7C). At 10.2 ns, the GPIbα β-switch had dissociated from the A1 central β-sheet, but the E14:R1334 interaction remained intact, as did a few other hydrophobic interactions (Figure 7D). At 10.8 ns, rupture of the E14:R1334 interaction led to complete dissociation of GPIbαN from A1 (Figure 7E). Figure 7F shows the rotation of A1 and the sliding of the GPIbα β-finger over A1.

These observations are similar to our previous SMD simulations of unbinding of the P-selectin:P-selectin glycoprotein ligand–1 (P-selectin:PSGL-1) complex (45), although the P-selectin:PSGL-1 structure is very different from the GPIbαN:A1 structure. The insights from our previous study allowed us to develop a sliding-rebinding model for selectin/ligand catch bonds, which was sup-

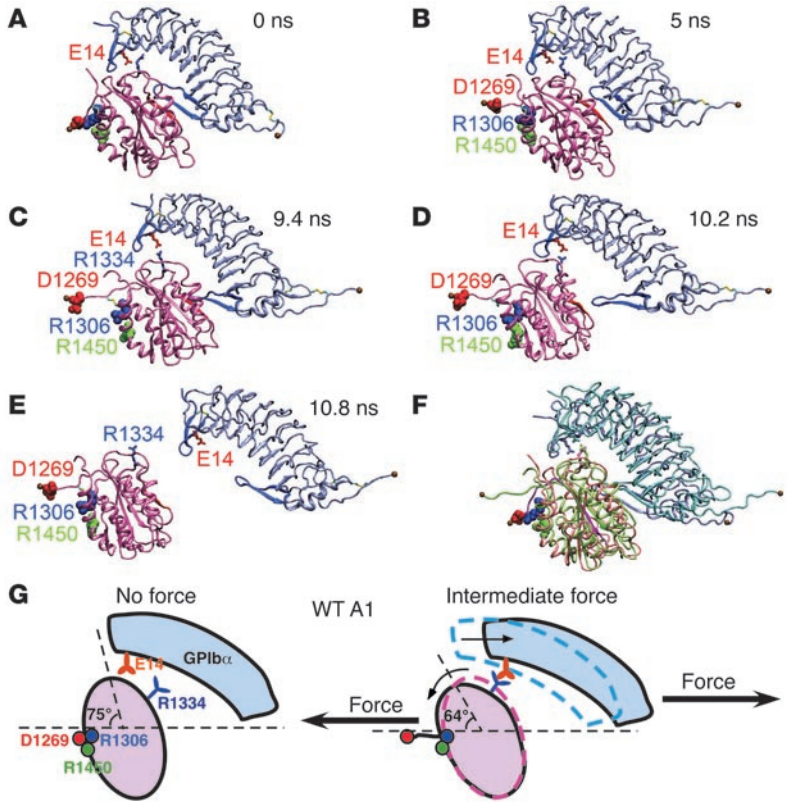

Figure 7
Structural model for WT A1 catch bonds (see Results for details). (**A**–**E**) Sequential snapshots of SMD-simulated structures showing pathways of the sliding-rebinding mechanism. Mauve, A1; gray, GPIbαN; red spheres, D1269; blue spheres, R1306; green spheres, R1450; blue β-strands, β-switch; red β-strands, central β-sheet of A1; red sticks, E14; blue sticks, R1334. The equilibrated structure (**A**) was used as a starting point of SMD simulations to generate the simulated structures in **B**–**E**. (**F**) Overlay of the structures in **A** (colors same as in **A**) and **D** (green, A1; cyan, GPIbα), showing the rotation of A1 and sliding of the GPIbα β-finger over A1. (**G**) Sliding-rebinding mechanism for GPIb/vWF A1 catch bonds.

ported by prior mutagenesis studies (30). Remarkably, the sliding-rebinding model was also applicable to GPIbα/vWF catch bonds (Figure 7G). At low forces, the salt bridge between D1269 and R1306/R1450 stabilizes the A1 orientation at 75° to horizontal. Dissociation occurs without engagement of GPIbα E14 with A1 R1334, which yields short lifetimes. At intermediate forces, rupture of the salt bridge between D1269 and R1306/R1450 extends the A1 N-terminal sequence, resulting in a torque to rotate A1 to 64° to horizontal. This allows the GPIbα β-finger to slide over the top surface of A1, during which GPIbα E14 forms a salt bridge with A1 R1334. This new interaction is formed after force is applied. It appears that this strong and long-lived new interaction prolongs lifetimes, which gives rise to catch bonds. Further increases in force do not form new interactions but instead disrupt existing interactions, converting catch bonds to slip bonds.

To understand the structural basis for why the R1306Q mutant exhibits a gain-of-function phenotype and how it converts catch bonds to slip bonds with prolonged lifetimes at low forces, we compared the structure of mutant M239V GPIbαN bound to mutant R1306Q A1 (13) with the structure of WT GPIbαN bound to WT A1 (Figure 8A) (14). The largest conformational change was seen in loop 1308–1314 that follows the mutated residue R1306Q in A1 (Figure 8A, boxed region). However, energy calculations (data not shown) did not support a previous suggestion that this conformational change increases binding affinity of the mutant A1 for GPIbα (13). By comparison, the side-chain of R1334 tilted leftward in the mutant structure, enabling it to contact E14 of GPIbα through 1 arm (Figure 8A, boxed region). During the equilibration preparation for SMD simulations, a salt bridge formed between mutant A1 R1334 and GPIbα E14 (Figure 8B, boxed region). However, no new contact was observed during SMD simulations (Supplemental Video 2). Thus, the E14:R1334 salt bridge formed at 0 force in the free SMD-simulated mutant structure but was induced by force in the SMD-simulated WT structure. These results explain the prolonged lifetimes of bonds of R1306Q A1 with GPIbα at low forces and the ordinary slip bond behavior of this interaction (Figure 8C).

The above model may apply to R1450E A1, because this mutation may also cause the E14:R1334 salt bridge to form at 0 force (Figure 8C). Alternatively, the R1450E substitution may eliminate the salt bridge(s) of residue 1306 and/or 1450 with D1269. This may allow the A1 N-terminal sequence to extend, the A1 domain to rotate, and the new E14:R1334 salt bridge to form at very low forces, which may prolong lifetimes and eliminate catch bonds (Figure 8D).

Discussion

Our findings demonstrate how force regulates platelet rolling on vWF, illustrate its similarity to force regulation of leukocyte rolling through selectins, suggest a structural basis for this regulation, and offer insights into the molecular basis for type 2B vWD. The counterintuitive requirement for arterial flows to support platelet adhesion to vWF was noted over a decade ago, but had not been explained (1, 19, 21). Previous studies reported that flow increases the tethering of flowing platelets to vWF and the number of platelets rolling on vWF (1, 19, 21). Tethering may be governed by the on-rate of formation of GPIbα/vWF bonds (46), whereas rolling depends on both on- and off-rates. Our present study demonstrates how flow strengthened rolling adhesion through slower and more regular rolling steps (Figures 1, 3, and 4), which were governed by the off-rate of dissociation of GPIbα/vWF bonds. First, by measuring force-dependent lifetimes of single bonds or tethers between purified or platelet-expressed GPIbα and vWF A1 domain at forces

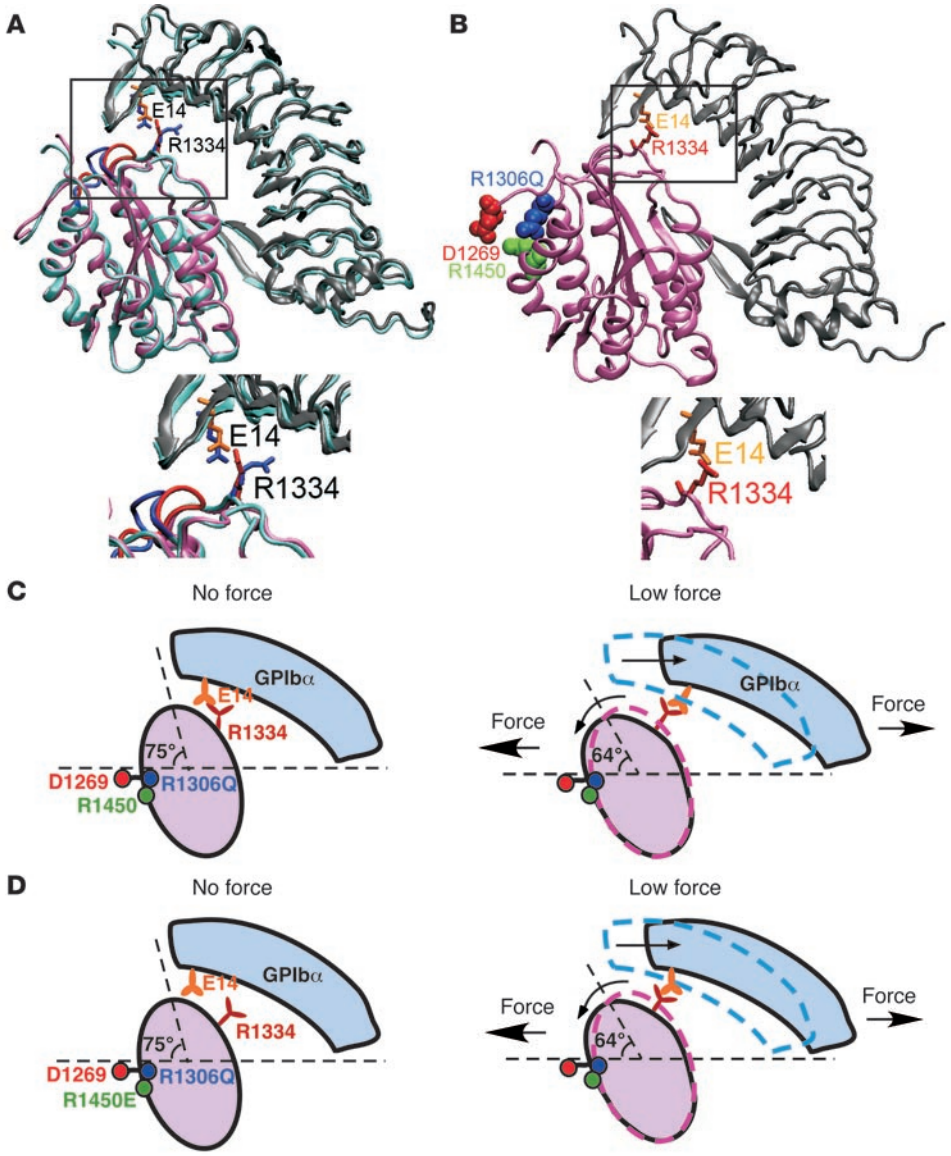

Figure 8
Structural models for elimination of catch bonds by A1 mutations (see Results for details). (**A**) Comparison of the mutant structure of GPIbαN (gray) liganded with A1 (pink) with the structure of the WT complex (cyan). The mutant structure includes substitutions in both GPIbαN (M239V) and A1 (R1306Q). The conformational changes observed in the 1308–1314 loop of A1 are highlighted in blue in the WT and red in the mutant structure (boxed region). The A1 residue R1334 in the WT structure (blue sticks) is tilted leftward in the mutant structure (red sticks), which reduces its distance to the GPIbα residue E14 in the mutant structure (orange sticks), but not in the WT structure (blue sticks). (**B**) After energy minimization, a salt bridge formed between A1 R1334 and GPIbα E14 in the mutant structure, which was held during most of the 20-ns equilibration simulations. This salt bridge did not form in the WT structure (see Figure 7). (**C**) Model for the R1306Q mutation to eliminate catch bonds. (**D**) Alternative model for the R1450E mutation to eliminate catch bonds.

lower than those previously studied (21, 23), we directly demonstrated transitions from catch bonds to slip bonds (Figure 2). Second, by scaling analysis of platelet and GPIbα-bearing microsphere rolling on intact vWF or vWF A1 domain (Figures 1, 3, and 4), we showed that force-dependent dissociation kinetics of GPIbα/vWF interactions governed rolling velocity and that catch bonds specifically governed flow-enhanced rolling, i.e., the ability to roll more slowly and more regularly as flow increases from a suboptimal rate. As flow increased above the optimal rate, catch bonds transitioned to slip bonds and rolling velocities increased. Interactions of P-selectin (27) and L-selectin (28) with their glycosylated ligands also transition from catch to slip bonds as force increases, and catch bonds govern flow-enhanced leukocyte rolling through L-selectin (29). Thus, 2 structurally distinct receptor/ligand systems use catch bonds to enable flow-enhanced rolling of blood cells on vascular surfaces.

We used 2 single-residue substitutions in the vWF A1 domain, R1306Q (32) and R1450E (33–35), to further explore the force regulation of GPIbα/vWF interactions. Both vWF mutants exhibit features of type 2B vWD, and both have increased affinity for GPIbα in the absence of force (13, 35). Extending this result, we observed that bond lifetimes of both A1 mutants with GPIbα were longer at low forces, eliminating catch bonds and resulting in a monotonic shortening of bond lifetimes (slip bonds) as force increased (Figure 2, C and D). These mutations eliminated the shear threshold requirement for platelet or GPIbα-bearing microsphere rolling on vWF (Figures 3 and 4) and strengthened the causal relationship between rolling velocity and the dissociation kinetics of GPIbα/vWF bonds. Single-residue substitutions in the hinge between the lectin and EGF domains of L-selectin (30) or in the ligand-binding surface of L-selectin (31) similarly prolong bond lifetimes at low forces and reduce (30) or eliminate (31) the shear threshold for leukocyte rolling. Catch bonds provide a mechanism to support platelet rolling on vWF immobilized on surfaces but prevent inappropriate agglutination of circulating platelets by binding to vWF multimers in plasma. Consistent with this notion, flowing platelets agglutinated with microspheres bearing R1306Q or R1450E A1 or R1450 A1A2A3 but not with WT A1 or WT A1A2A3 (Figure 6). Similarly, flowing leukocytes, which express the L-selectin

ligand PSGL-1, do not agglutinate with microspheres bearing WT L-selectin but do agglutinate with microspheres bearing L-selectin mutants that prolong lifetimes at low forces (30). Thus, catch bonds may provide a general mechanism for blood cells to adhere to vascular surfaces but not to agglutinate as they circulate.

Crystal structures of GPIbα/vWF A1 complexes have provided important information on the molecular details of the interactions (13, 14), but do not indicate how the complexes respond to applied force and have not readily explained how type 2B vWD mutations in the A1 domain clustered outside the binding site can alter function. Our SMD simulations of dissociation of the WT GPIbαN:A1 complex (Figure 7 and Supplemental Video 1) enabled us to visualize dynamic conformations not seen in the equilibrium conformations of the crystal structures, to determine how force regulates these conformational changes, and to assess how such changes might elicit catch bonds. These simulations suggest that force breaks interactions of D1269 with R1306 or R1450 in the A1 domain, causing A1 to rotate and slide along the interface with GPIbα. The sliding allows R1334 in A1 to form a strong salt bridge with E14 in GPIbα that delays dissociation of the molecular complex after all atomic-level interactions seen in the crystal structure have disrupted. This provides a structural mechanism for the experimentally observed catch bonds. Remarkably, the sliding-rebinding mechanism resembles that observed in SMD simulations of P-selectin dissociating from its ligand PSGL-1, where force breaks interactions at the lectin–EGF domain interface, causing the lectin domain to rotate and to form new interactions as it slides along the interface with PSGL-1 (45). A mutation that disrupts an interaction between the lectin and EGF domains of L-selectin reduces the force required to rotate the lectin domain and to slide along the interface with its ligands (30).

Our free dynamics and SMD simulations of dissociation of the mutant GPIbαN:A1 complex (Figure 8 and Supplemental Video 2) have provided explanations for the gain-of-function phenotype of and the elimination of catch bonds by the R1306Q mutation, which may also explain the effects of the R1450E mutation. In this model, the mutation results in formation of the E14:R1334 salt bridge at 0 force and no new contacts after force is applied. An alternative model similar to one previously proposed (30) suggests that the R1450E mutation removes the interaction with D1269, which allows the sliding-rebinding mechanism to allosterically prolong lifetimes at forces near 0. The same mechanism can explain the gain-of-function phenotype of the H1268A/D1269A A1 mutant (16), because the D1269A substitution also eliminates the salt bridge(s) with R1306 and R1450. Our SMD simulations explained the loss-of-function phenotype of the type 2M vWD A1 mutant R1334A (47), which would prevent this residue from forming a salt bridge with GPIbα E14 during sliding and thus would not delay dissociation. Residues 1268 and 1269 reside in the linker region between the D3 and A1 domains. This linker and/or the D3 domain itself may form noncovalent contacts with A1. These contacts may allow the D3 and/or other domains to regulate the forced dissociation of A1 from GPIbα in a manner similar to that of the salt bridges between D1269 and R1306/R1450. This may explain why deleting the D′D3 region augments binding to GPIbα and adding an isolated D′D3 region inhibits GPIbα binding to vWF lacking this region (48). Deleting the D′D3 region (residues 764–1259) may affect the D1269:R1306/R1450 salt bridges, causing a gain-of-function phenotype like that of R1450E A1. The isolated D′D3 region (residues 764–1247) may still interact with vWF lacking this region via the same noncovalent contacts, which may reestablish some of the interactions between D′D3 and A1 that enable catch bonds. Further experiments and SMD simulations are required to test these predictions and to elucidate how other mutations of A1 alter function in type 2B or type 2M vWD.

Our data provide a biophysical mechanism for the phenotype of patients with type 2B vWD. The platelet-binding activity of vWF increases with the size of multimers, which may assume different conformations to expose binding sites for GPIbα on A1 domains (49, 50). In thrombotic thrombocytopenic purpura, ultralarge multimers may be particularly capable of exposing very large numbers of binding sites on A1 domains that spontaneously agglutinate circulating platelets (51). However, the number of exposed binding sites in plasma vWF multimers of normal size cannot stably agglutinate platelets, because the lifetimes of A1 bonds with GPIbα are too short at arterial shear rates (500–5,000 s^{-1}). Shear-induced platelet aggregation only occurs at the very high shear rates, such as 20,000 s^{-1}, found in stenotic arteries (15, 38). At these shear rates, the forces applied to platelet doublets linked by vWF multimers are sufficiently large to elicit catch bonds (Figure 5B), which prolong bond lifetimes enough to agglutinate circulating platelets. Extremely high shear rates may also expose more binding sites for GPIbα on A1 domains of normal-sized multimers (15, 38). In type 2B vWD, the longer lifetimes of vWF with GPIbα at low forces enable plasma vWF multimers to bind stably to circulating platelets. This explains the ability of these vWF mutants to spontaneously agglutinate platelets in vitro at shear rates as low as 200 s^{-1} or in response to low concentrations of a modulator such as ristocetin (52). Our present data demonstrated that the mutations directly affect the mechanical properties of isolated A1 domain bonds with GPIbα, but they do not exclude an additional effect of the mutations to expose more A1 domains on vWF multimers. In vivo, the enhanced binding also agglutinates platelets, which depletes larger vWF multimers from plasma and may cause thrombocytopenia. Furthermore, flow exerts force on the vWF that agglutinates platelets, exposing the cleavage site for the protease ADAMTS-13 (Figure 6G) and further reducing the larger vWF multimers (42, 44). Bleeding results from depletion of larger vWF multimers from plasma, limiting their availability for binding to collagen on disrupted vascular surfaces, and from occupancy of GPIbα by plasma vWF, preventing interactions with collagen-bound vWF.

Methods

Proteins and antibodies. Glycocalicin (the extracellular portion of GPIbα) was purified from human platelets as previously described (53). Recombinant ADAMTS-13 was produced as described previously (54). Recombinant WT A1, R1306Q A1, R1450E A1, and WT A1A2A3 were produced as described previously (10, 35, 55). Recombinant R1450E A1A2A3 was expressed in HEK293 cells and purified from conditioned medium similarly to WT A1A2A3.

Mouse anti-A1 mAbs 5D2 and 6G1 and anti-GPIbα mAb WM23, which recognizes the macroglycopeptide region, were gifts from M. Berndt (Monash University, Melbourne, Victoria, Australia). Mouse anti-A1 mAb AVW-3 was purchased from GTI. Mouse anti-GPIbα mAb AK2 and biotin-conjugated anti-CD61 mAb were purchased from Chemicon. PE-conjugated anti-CD61 mAb was purchased from BD Biosciences — Pharmingen. Alexa Fluor 555–conjugated streptavidin was purchased from Invitrogen. Fluoresbrite Yellow-Green–labeled microspheres (3-μm radius) were purchased from Polysciences.

AFM single-bond lifetime measurements. A previously described custom-made AFM was used to measure lifetimes of GPIbα/vWF A1 bonds (27). To reduce nonspecific binding, a polystyrene Petri dish was washed with absolute ethanol and dried with argon gas. WT or mutant A1 (15 μl; 10 μg/ml) was incubated on each of 2 spots on the Petri dish at 4°C overnight. The Petri dish

was washed 3 times with PBS and blocked with PBS containing 1% BSA. AFM cantilevers were soaked in PBS containing 1% BSA (for negative control) or 10 μg/ml glycocalicin at 4°C overnight. Lifetimes of GPIbα/A1 bonds were measured in thousands of repeated test cycles. Each cycle consisted of moving the cantilever tip to touch the Petri dish for 0.02 s; retracting it approximately 4 nm above the surface; holding it for 1 s to allow for bond formation; further retracting it a predetermined distance to see whether binding occurs; if so, determining whether the bond survives ramping to the preset force; if so, measuring how long the bond lasts at that force (i.e., bond lifetime); and finally retracting it to the starting position. Suspending the cantilever tip approximately 4 nm above the surface in the bond formation phase usually reduced nonspecific binding to less than 5% of the test cycles, whereas specific GPIb/A1 binding occurred in approximately 20% of the test cycles (31).

Platelet purification. Platelet-rich plasma was prepared from blood collected from healthy donors in 1:10 citrate buffer (170 mM sodium citrate and 83 mM citric acid in water) according to a protocol approved by the Institutional Review Board of the Oklahoma Medical Research Foundation. Blood was centrifuged at 150 *g* for 15 min at room temperature. Platelet-rich plasma was then centrifuged at 900 *g* for 5 min. The platelet pellet was resuspended in HEPES-Tyrode buffer (134 mM sodium chloride, 12 mM sodium bicarbonate, 2.9 mM potassium chloride, 0.34 mM sodium phosphate monobasic, 5 mM HEPES, and 5 mM glucose, pH 7.4). In some experiments, platelets were fixed with 1% paraformaldehyde for 20 min at room temperature.

Platelet lysates. Platelets (2×10^9) were pelleted and resuspended in 5 ml lysis buffer (2% Triton, 100 mM sodium chloride, 20 mM Tris, 5 mM benzamidine, 5 mM EDTA, and 100 μM leupeptin) at 4°C for 30 min with stirring. After centrifugation at 4°C for 20 min at 16,000 *g*, the supernatant was removed and concentrated using a centrifugal filter (50 K; Millipore).

Coating GPIbα onto microspheres. Polystyrene microspheres with 1- or 3-μm radii (10^8 or 10^7; Polysciences) were incubated with 200 μg/ml anti-mouse IgG Fc antibody (Chemicon) in HBSS overnight at 4°C. Microspheres were washed with HBSS, incubated with 1% HSA in HBSS for 2 h at room temperature to block nonspecific binding, and then incubated with 50 μg/ml anti-GPIbα mAb WM23 for 2 h at 4°C. After washing with HBSS, the microspheres were incubated with platelet lysates for 2 h at 4°C with occasional vortexing. After incubation, which captured GPIbα through binding to mAb WM23, the microspheres were washed with HBSS and resuspended in PBS with 0.5 % HSA.

Flow assay. Microspheres or platelets were perfused at various flow rates over WT vWF (coated at 100 or 440 μg/ml) or WT, R1306Q, or R1450E vWF A1 (coated at 50 μg/ml) in a parallel-plate flow chamber. To increase the viscosity by 2.6-fold in some experiments, Ficoll was added to the medium to a final concentration of 6% (w/v). In some experiments, microspheres or platelets were perfused in medium containing 20 μg/ml anti-GPIbα mAb AK2 to block binding to vWF. All binding events were specific because they were eliminated by inclusion of mAb. Mean rolling velocities were measured over a 1-s interval by video microscopy with frame-by-frame particle-tracking software at 250 fps. Site densities of vWF were determined by binding of ^{125}I-labeled anti-vWF mAb AVW-3.

Transient tether lifetimes of platelets or 1-μm-radius microspheres bearing GPIbα were measured on low densities of WT A1 (coated at 2 μg/ml) that did not support rolling or skipping at any wall shear stress (29). Images captured at 250 fps were replayed in slow motion, and duration of transient tethers was measured using frame-by-frame analysis. At each wall shear stress, approximately 100 events of platelets or microspheres tethering were measured and averaged. Data are presented as mean ± SD of the 3 independent sets of average lifetimes.

Calculations of tensile forces between a sphere and a wall or between 2 spheres in a doublet. To relate wall shear stress to force tethering a sphere to a wall, we measured lever arms as described previously (37). Microspheres of 3-μm radius bearing GPIbα were allowed to tether to low-density R1450E A1 in flow-reversal experiments performed at 5 wall shear stresses ranging from 0.2 to 1.2 dyn/cm^2. The measured lever arm was 1.43 ± 0.3 μm (mean ± SD, 10 measurements at each wall shear stress). This allowed us to calculate the conversion factor between wall shear stress and tether force: 88 pN per dyn/cm^2. The conversion factor for the 1-mm-radius microspheres is 9.7 pN per dyn/cm^2, 9-fold smaller than that of the 3-μm-radius microspheres, based on a previously determined similarity equation, which states that the tether force is proportional to the square of microsphere radius, provided that tethering is mediated by the same molecular interaction (29). The average tensile force (F_t) between 2 spheres of respective radii r_1 and r_2 separated by a gap of distance h in a doublet tumbling in a fluid of viscosity of μ sheared by shear rate G was calculated from fluid mechanics theory: $F_t = (\alpha\mu/\pi)r_1r_2G$, where α is a weak function of h/r_1 and h/r_2 (40). If h is 60 nm, r_1 and r_2 equal 1 μm, and μ is 10^{-3} N/m^2, then $\alpha\mu/\pi$ equals 6.2×10^{-3} s/μm^2. If other parameters are the same but r_2 increases to 3 μm, this coefficient is reduced to 4.7×10^{-3} s/μm^2.

Agglutination assay of flowing microspheres and platelets. Unlabeled or Yellow-Green–labeled 3-μm microspheres were coated with WT A1, R1306Q A1, R1450E A1, WT A1A2A3, or R1450E A1A2A3. After blocking with HBSS plus 1% HSA, A1-coated microspheres (10^6/ml) were mixed with isolated platelets (10^8/ml) in HEPES-Tyrode buffer with 0.5 % HSA. The platelet/microsphere mixtures were perfused through a flow chamber coated with 1% HSA at a wall shear rate of 100 s^{-1}. In some experiments, A1A2A3-coated microspheres were incubated in the presence or absence of 5 μg/ml recombinant ADAMTS-13. Platelet/microsphere mixtures in HEPES-Tyrode buffer containing 5 mM $CaCl_2$ and 0.1 μM $ZnCl_2$ (44) were perfused through a flow chamber at wall shear rates ranging from 100 s^{-1} to 2,000 s^{-1} with or without 10 mM EDTA. After exiting the flow chamber, samples were collected and fixed with 1% paraformaldehyde. For flow cytometric analysis, samples were stained by PE-conjugated anti-CD61 mAb to detect platelet binding on the microspheres. For immunofluorescence microscopic analysis, samples were incubated with biotin-conjugated anti-CD61 mAb and stained with Alexa Fluor 555–conjugated streptavidin.

SMD simulations. SMD simulations were performed using the NAMD program (56) with the CHARMM22 all-atom force field for protein (57). The X-ray crystal structure of the WT (Protein Data Bank code 1SQ0; ref. 14) or mutant (Protein Data Bank code 1M10; ref. 13) GPIbα/vWF A1 complex was used as the initial structure, which was put in a 160 Å × 96 Å × 72 Å water box with 9 (for the mutant structure) or 10 (for the WT structure) Na^+ and 21 Cl^- ions to neutralize the system, which contained 140,570 atoms. The system was subjected to 10,000 steps of energy minimization with heavy atoms fixed and another 10,000 steps with all atoms free. The system was heated gradually from 0°K to 300°K in 0.1 ns and then equilibrated for 3 ns with pressure and temperature control. The temperature was held at 300°K using Langevin dynamics, and the pressure was held at 1 atm by the Langevin piston method. The equilibrated structure was taken as the starting point for SMD simulations. In SMD, the C_α atom of the A1 N-terminal residue H1268 was harmonically constrained and the C_α atom of the GPIbα C-terminal residue L267 was pulled at a constant speed of approximately 0.5 nm/ns with spring constant of about 700 pN/nm. The peak force is 1,000 pN, about 4-fold the largest force used in our experiments. We adjusted loading speeds and spring constants in order to accelerate the processes, so that unbinding could be observed in 10–15 ns of the simulation time. Structures in Figures 7 and 8 and Supplemental Videos 1 and 2 were generated using VMD (58).

Statistics. Data from AFM and flow chamber experiments are shown as mean ± SEM and mean ± SD, respectively. The number of measurements or experiments averaged is indicated in the figure legends. Changes in the percentage of CD61-positive A1A2A3 beads were analyzed by 2-tailed Student's *t* test (Microsoft Excel). A P value less than 0.05 was considered significant.

Acknowledgments

We thank Michael Berndt for providing anti-A1 (5D2 and 6G1) and anti-GPIbα (WM23) mAbs, Prasenjit Guchhait for the purification of glycocalicin, Cecilia Martin for the expression and purification of the recombinant A1 domain variants, Chalmette Ball for the expression and purification of ADAMTS-13, and Fang Kong for programming of the AFM force-clamp routine. The computational resources for SMD simulations were provided by IHPCL Laboratory of the College of Computing, Georgia Institute of Technology. This work was supported by NIH grants HL091020 (to C. Zhu), HL34363 and HL090923 (to R.P. McEver), HL072886 (to M.A. Cruz), HL71895 (to J.-F. Dong), P50HL065967 (to J.A. López), and HL18672 (to L.V. McIntire) and by a Scientist Development Grant from the American Heart Association (to J. Lou).

Received for publication March 26, 2008, and accepted in revised form July 9, 2008.

Address correspondence to: Cheng Zhu, Coulter Department of Biomedical Engineering, Georgia Institute of Technology, 315 Ferst Drive, Atlanta, Georgia 30332, USA. Phone: (404) 894-3269; Fax: (404) 385-1397; E-mail: cheng.zhu@bme.gatech.edu. Or to: Rodger P. McEver, Cardiovascular Biology Research Program, Oklahoma Medical Research Foundation, 825 NE 13th Street, Oklahoma City, Oklahoma 73104, USA. Phone: (405) 271-6480; Fax: (405) 271-3137; E-mail: rodger-mcever@omrf.org.

Tadayuki Yago, Jizhong Lou, and Tao Wu contributed equally to this work.

1. Savage, B., Saldivar, E., and Ruggeri, Z.M. 1996. Initiation of platelet adhesion by arrest onto fibrinogen or translocation on von Willebrand factor. *Cell.* **84**:289–297.
2. Weiss, H.J. 1975. Platelet physiology and abnormalities of platelet function. *N. Engl. J. Med.* **293**:580–588.
3. Fuster, V., Badimon, L., Badimon, J.J., and Chesebro, J.H. 1992. The pathogenesis of coronary artery disease and the acute coronary syndromes I. *N. Engl. J. Med.* **326**:242–250.
4. Fuster, V., Badimon, L., Badimon, J.J., and Chesebro, J.H. 1992. The pathogenesis of coronary artery disease and the acute coronary syndromes II. *N. Engl. J. Med.* **326**:310–318.
5. McEver, R.P. 2001. Adhesive interactions of leukocytes, platelets, and the vessel wall during hemostasis and inflammation. *Thromb. Haemost.* **86**:746–756.
6. Moake, J.L. 2002. Thrombotic thrombocytopenic purpura: the systemic clumping "plague". *Annu. Rev. Med.* **53**:75–88.
7. Sadler, J.E., et al. 2006. Update on the pathophysiology and classification of von Willebrand disease: a report of the Subcommittee on von Willebrand Factor. *J. Thromb. Haemost.* **4**:2103–2114.
8. Verweij, C.L., Diergaarde, P.J., Hart, M., and Pannekoek, H. 1986. Full-length von Willebrand factor (vWF) cDNA encodes a highly repetitive protein considerably larger than the mature vWF subunit. *EMBO J.* **5**:1839–1847.
9. Cruz, M.A., Handin, R.I., and Wise, R.J. 1993. The interaction of the von Willebrand factor-A1 domain with platelet glycoprotein Ib/IX. The role of glycosylation and disulfide bonding in a monomeric recombinant A1 domain protein. *J. Biol. Chem.* **268**:21238–21245.
10. Cruz, M.A., Diacovo, T.G., Emsley, J., Liddington, R., and Handin, R.I. 2000. Mapping the glycoprotein Ib-binding site in the von willebrand factor A1 domain. *J. Biol. Chem.* **275**:19098–19105.
11. López, J.A., et al. 1987. Cloning of the alpha chain of human platelet glycoprotein Ib: a transmembrane protein with homology to leucine rich alpha2-glycoprotein. *Proc. Natl. Acad. Sci. U. S. A.* **84**:5615–5619.
12. Berndt, M.C., Shen, Y., Dopheide, S.M., Gardiner, E.E., and Andrews, R.K. 2001. The vascular biology of the glycoprotein Ib-IX-V complex. *Thromb. Haemost.* **86**:178–188.
13. Huizinga, E.G., et al. 2002. Structures of glycoprotein Ibα and its complex with von Willebrand factor A1 domain. *Science.* **297**:1176–1179.
14. Dumas, J.J., et al. 2004. Crystal structure of the wild-type von Willebrand factor A1-glycoprotein Ibα complex reveals conformation differences with a complex bearing von Willebrand disease mutations. *J. Biol. Chem.* **279**:23327–23334.
15. Dong, J.F., et al. 2001. Ristocetin-dependent, but not botrocetin-dependent, binding of von Willebrand factor to the platelet glycoprotein Ib-IX-V complex correlates with shear-dependent interactions. *Blood.* **97**:162–168.
16. Matsuhita, T., and Sadler, J.E. 1995. Identification of amino acid residues essential for von Willebrand factor binding to platelet glycoprotein Ib. *J. Biol. Chem.* **270**:13406–13414.
17. Sadler, J.E. 2005. New concepts in von Willebrand disease. *Annu. Rev. Med.* **56**:173–191.
18. Kroll, M.H., Hellums, J.D., McIntire, L.V., Schafer, A.I., and Moake, J.L. 1996. Platelets and shear stress. *Blood.* **88**:1525–1541.
19. Doggett, T.A., et al. 2003. Alterations in the intrinsic properties of the GPIbα-VWF tether bond define the kinetics of the platelet-type von Willebrand disease mutation, Gly233Val. *Blood.* **102**:152–160.
20. Federici, A.B., et al. 1997. A type 2b von Willebrand disease mutation (Ile546 3 Val) associated with an unusual phenotype. *Thromb. Haemost.* **78**:1132–1137.
21. Doggett, T.A., et al. 2002. Selectin-like kinetics and biomechanics promote rapid platelet adhesion in flow: the GPIbα-vWF tether bond. *Biophys. J.* **83**:194–205.
22. Chen, S.Q., Alon, R., Fuhlbrigge, R.C., and Springer, T.A. 1997. Rolling and transient tethering of leukocytes on antibodies reveal specializations of selectins. *Proc. Natl. Acad. Sci. U. S. A.* **94**:3172–3177.
23. Kumar, R.A., et al. 2003. Kinetics of GPIbα-vWF-A1 tether bond under flow: effect of GPIbα mutations on the association and dissociation rates. *Biophys. J.* **85**:4099–4109.
24. Alon, R., Hammer, D.A., and Springer, T.A. 1995. Lifetime of the P-selectin: carbohydrate bond and its response to tensile force in hydrodynamic flow. *Nature.* **374**:539–542.
25. Alon, R., Chen, S.Q., Puri, K.D., Finger, E.B., and Springer, T.A. 1997. The kinetics of L-selectin tethers and the mechanics of selectin-mediated rolling. *J. Cell Biol.* **138**:1169–1180.
26. Zhu, C., Yago, T., Lou, J., Zarnitsyna, V.I., and McEver, R.P. 2008. Mechanisms for flow-enhanced cell adhesion. *Ann. Biomed. Eng.* **36**:604–621.
27. Marshall, B.T., et al. 2003. Direct observation of catch bonds involving cell-adhesion molecules. *Nature.* **423**:190–193.
28. Sarangapani, K.K., et al. 2004. Low force decelerates L-selectin dissociation from P-selectin glycoprotein ligand-1 and endoglycan. *J. Biol. Chem.* **279**:2291–2298.
29. Yago, T., et al. 2004. Catch bonds govern adhesion through L-selectin at threshold shear. *J. Cell Biol.* **166**:913–923.
30. Lou, J., et al. 2006. Flow-enhanced adhesion regulated by a selectin interdomain hinge. *J. Cell Biol.* **174**:1107–1117.
31. Klopocki, A.G., et al. 2008. Replacing a lectin-domain residue in L-selectin enhances binding to P-selectin glycoprotein ligand-1 but not to 6-sulfosialyl Lewis x. *J. Biol. Chem.* **283**:11493–11500.
32. Lankhof, H., et al. 1997. Functional studies on platelet adhesion with recombinant von Willebrand factor type 2B mutants R543Q and R543W under conditions of flow. *Blood.* **89**:2766–2772.
33. Matsushita, T., and Sadler, J.E. 1995. Identification of amino acid residues essential for von Willebrand factor binding to platelet glycoprotein Ib. Charged-to-alanine scanning mutagenesis of the A1 domain of human von Willebrand factor. *J. Biol. Chem.* **270**:13406–13414.
34. de Romeuf, C., Hilbert, L., and Mazurier, C. 1998. Platelet activation and aggregation induced by recombinant von Willebrand factors reproducing four type 2B von Willebrand disease missense mutations. *Thromb. Haemost.* **79**:211–216.
35. Morales, L.D., Martin, C., and Cruz, M.A. 2006. The interaction of von Willebrand factor-A1 domain with collagen: mutation G1324S (type 2M von Willebrand disease) impairs the conformational change in A1 domain induced by collagen. *J. Thromb. Haemost.* **4**:417–425.
36. Mody, N.A., et al. 2005. Mechanics of transient platelet adhesion to von Willebrand factor under flow. *Biophys. J.* **88**:1432–1443.
37. Yago, T., et al. 2002. Distinct molecular and cellular contributions to stabilizing selectin-mediated rolling under flow. *J. Cell Biol.* **158**:787–799.
38. Ruggeri, Z.M., Orje, J.N., Habermann, R., Federici, A.B., and Reininger, A.J. 2006. Activation-independent platelet adhesion and aggregation under elevated shear stress. *Blood.* **108**:1903–1910.
39. Szanto, T., et al. 2007. Type 2B von Willebrand disease in seven individuals from three different families: phenotypic and genotypic characterization. *Thromb. Haemost.* **98**:251–254.
40. Shankaran, H., and Neelamegham, S. 2004. Hydrodynamic forces applied on intercellular bonds, soluble molecules, and cell-surface receptors. *Biophys. J.* **86**:576–588.
41. Goldman, A.J., Cox, R.G., and Brenner, H. 1967. Slow viscous motion of a sphere parallel to a plane wall — Couette flow. *Chem. Eng. Sci.* **22**:653–660.
42. Tsai, H.M., Sussman, I.I., and Nagel, R.L. 1994. Shear stress enhances the proteolysis of von Willebrand factor in normal plasma. *Blood.* **83**:2171–2179.
43. Dong, J.F., et al. 2002. ADAMTS-13 rapidly cleaves newly secreted ultralarge von Willebrand factor multimers on the endothelial surface under flowing conditions. *Blood.* **100**:4033–4039.
44. Shim, K., Anderson, P.J., Tuley, E.A., Wiswall, E., and Sadler, J.E. 2008. Platelet-VWF complexes are preferred substrates of ADAMTS13 under fluid shear stress. *Blood.* **111**:651–657.
45. Lou, J., and Zhu, C. 2007. A structure-based sliding-rebinding mechanism for catch bonds. *Biophys. J.* **92**:1471–1485.
46. Yago, T., Zarnitsyna, V.I., Klopocki, A.G., McEver, R.P.,

and Zhu, C. 2007. Transport governs flow-enhanced cell tethering through L-selectin at threshold shear. *Biophys. J.* **92**:330–342.
47. Matsushita, T., Meyer, D., and Sadler, J.E. 2000. Localization of von Willebrand factor-binding sites for platelet glycoprotein Ib and botrocetin by charged-to-alanine scanning mutagenesis. *J. Biol. Chem.* **275**:11044–11049.
48. Ulrichts, H., et al. 2006. Shielding of the A1 domain by the D'D3 domains of von Willebrand factor modulates its interaction with platelet glycoprotein Ib-IX-V. *J. Biol. Chem.* **281**:4699–4707.
49. Siedlecki, C.A., et al. 1996. Shear-dependent changes in the three-dimensional structure of human von Willebrand factor. *Blood.* **88**:2939–2950.
50. Hulstein, J.J., et al. 2005. A novel nanobody that detects the gain-of-function phenotype of von Willebrand factor in ADAMTS13 deficiency and von Willebrand disease type 2B. *Blood.* **106**:3035–3042.
51. Moake, J.L., and Chow, T.W. 1998. Increased von Willebrand factor (vWf) binding to platelets associated with impaired vWf breakdown in thrombotic thrombocytopenic purpura. *J. Clin. Apher.* **13**:126–132.
52. Ruggeri, Z.M., Pareti, F.I., Mannucci, P.M., Ciavarella, N., and Zimmerman, T.S. 1980. Heightened interaction between platelets and factor VIII/von Willebrand factor in a new subtype of von Willebrand's disease. *N. Engl. J. Med.* **302**:1047–1051.
53. Romo, G.M., et al. 1999. The glycoprotein Ib-IX-V complex is a platelet counterreceptor for P-selectin. *J. Exp. Med.* **190**:803–814.
54. Tao, Z., et al. 2005. Recombinant CUB-1 domain polypeptide inhibits the cleavage of ULVWF strings by ADAMTS13 under flow conditions. *Blood.* **106**:4139–4145.
55. Auton, M., Cruz, A.A., and Moake, J.L. 2006. Conformational stability and domain unfolding of the von Willebrand factor A domains. *J. Mol. Biol.* **366**:986–1000.
56. Phillips, J.C., et al. 2005. Scalable molecular dynamics with NAMD. *J. Comput. Chem.* **26**:1781–1802.
57. MacKerell, A.D., Jr., et al. 1998. All-atom empirical potential for molecular modeling and dynamics studies of proteins. *J. Phys. Chem. B.* **102**:3586–3616.
58. Humphrey, W., Dalke, A., and Schulten, K. 1996. VMD-visual molecular dynamics. *J. Mol. Graph.* **14**:33–38.